Materials Chemistry and Physics 179 (2016) 120–128

Contents lists available at ScienceDirect

Materials Chemistry and Physics

journal homepage: www.elsevier.com/locate/matchemphys

A comprehensive study on step-wise surface modification of C_{60}: Effect of oxidation and silanization on dynamic mechanical and thermal stability of epoxy nanocomposite

Subhankar Das [a], Sudipta Halder [a, *], Kaushal Kumar [b]

[a] Department of Mechanical Engineering, National Institute of Technology Silchar, Silchar, 788010, Assam, India
[b] Department of Metallurgical and Materials Engineering, Indian Institute of Technology Roorkee, Roorkee, 247667, India

HIGHLIGHTS

- Stepwise modification was done to prepare silanized C_{60} (S-Fs).
- Silanization of C_{60} is demonstrated from a comprehensive physical characterization.
- Epoxy nanocomposites with blends of step-wise modified C_{60} were prepared.
- S-Fs confirms its potentiality to enhance stiffness and molecular relaxation of epoxy.
- Storage modulus was improved by ~491% for S-FEC without affecting their thermal stability.

ARTICLE INFO

Article history:
Received 9 February 2016
Received in revised form
22 April 2016
Accepted 27 April 2016

Keywords:
Composite materials
Fullerenes
Dynamic mechanical analyses
Thermogravimetric analysis

ABSTRACT

Fullerenes (C_{60}) are regarded as exceptional reinforcing material in composites for their capability to enrich multi-functional properties. In the present work, pristine C_{60} has been stepwise modified through oxidation in the presence of nitric acid and then silanized using 3-aminopropyltriethoxysilane (APTES) to generate oxygenated and siloxane functional group elements onto their surfaces. The morphological investigation of oxidized and silanized C_{60} was done under FESEM and TEM. On the other hand, FTIR spectroscopy and TGA analysis confirms the attachment of oxygenated and siloxane functional groups. The increase in structural defect, creating sites for APTES grafting is evident from Raman spectroscopy. Epoxy nanocomposites were prepared by incorporating 0.5 wt% of pristine and stepwise modified C_{60}. The effect of surface modification of C_{60} on epoxy nanocomposite is studied under DMA and TGA. The silanized C_{60}/epoxy nanocomposite showed significant enhancement of storage modulus (~491%) and enhanced intensity of tan δ peak compared to the neat epoxy. This is mainly attributed to high energy absorption during viscoelastic motion. From the TGA, silanized C_{60}/epoxy nanocomposite showed modest increment in initial decomposition temperature. This behavior is suggestive for potential espousal of silanized C_{60} to enhance the stiffness and molecular relaxation of epoxy nanocomposites.

1. Introduction

Incorporation of nanofillers for substantial improvement in mechanical and non-mechanical properties of polymer composites is an exciting avenue to prepare high performance advanced materials. Various fields of interest such as structural, optical, batteries, nanoelectronics and photovoltaic devices generates the compulsion to develop carbon nanofiller based polymer composites [1–3]. In this perspective, numerous research have been performed to develop polymer nanocomposites with different carbon nanofillers such as carbon nanotubes (CNTs) [4–6], carbon nanofiber (CNFs) [1], carbon nano bead [7] and graphene [8]. However, substantial influence on mechanical, thermo-mechanical, thermal and electrical properties improvement can be possible provided a good dispersion and interaction of the nanofillers with polymer network is achieved [9–11]. It has been found that, in comparison to other carbon nanofillers, the application of C_{60} as nanofiller is expected to uplift the polymer composite properties mainly due to

* Corresponding author.
E-mail address: shalder@nits.ac.in (S. Halder).

http://dx.doi.org/10.1016/j.matchemphys.2016.04.085
0254-0584/

non-entangling behavior and enhanced interfacial interaction through free radical scavenging and chain reaction termination [12]. In this regard, property variation of polymer composites having C_{60} as filler has been endorsed from limited research. Few works showed the use of low concentration of pristine C_{60} to influence the composite properties mainly attributed to trapping of free radicals associated with C_{60} [2,3,13–16]. However, enhancement in loading of C_{60} in polymer network is found to have negligible effect [16–18]. This might have happened due to tendency of nanofiller agglomeration at high concentration [17,19,20]. Hence, attempts were further made by others to use the antioxidant property of pristine C_{60} to reduce their oxidation behavior [14,21]. Many mechanisms have been suggested thereof, such as strong radical accepting capability, reduced initiation, inhibition of thermo-oxidation of C_{60} in various polymers that affects the properties [14,21]. However, challenges to overcome the self-aggregation tendency of C_{60} is still dominant and a challenge. To overcome such challenges of carbon nanofiller agglomeration in epoxy network, major effort is made on functionalization of CNTs [22,23], CNFs [24,25] and graphene [26]. These efforts demonstrates improvement in interfacial interaction between the functionalized carbon nanofillers with epoxy network by covalent or non-covalent linkages. Although, the non-covalent linkages improves the dispersion of the nanofillers in epoxy network but, a depression in storage modulus and other properties are observed [27]. On the other hand, covalent linkages signifies its potential to improve the properties of the epoxy nanocomposites [25,26], possibly due to the formation of two phase interfacial material at juncture of the nanofiller and epoxy network [24,25,28,29]. This gives us the essence of organically modified C_{60} to influence the thermo mechanical behavior of epoxy nanocomposite. 3-aminopropyltriethoxysilane (APTES) is a tremendously preferred silane coupling agents used for functionalizing nanofillers to tailor their interfacial interaction [24,29–32]. Tayfun et al. [31] showed a twofold enhancement in mechanical properties of thermoplastic polyurethane when, incorporated with silanized C_{60} at low concentration. At this end, and in comparison to other carbon nanomaterials such as CNTs [33], CNFs [34] and graphene [35], the full potential of functionalized C_{60} in polymer nanocomposites is yet to be explored. Moreover, it's a challenge to overcome the self-aggregation tendency of C_{60}, which causes poor miscibility in epoxy network [36]. The improved dispersion behavior of C_{60} in epoxy network can be achieved by generating non-covalent linkages onto C_{60}, similar to other carbon nanomaterials [37–39]. The dispersion behavior can be further modified if organic modification of oxidized C_{60} is performed to achieve covalent linkages between epoxy and C_{60}. To the best of author's knowledge, limited works elucidates the effect of oxidation and silanization of C_{60} on thermo-mechanical and thermal stability of the epoxy nanocomposites. This limited reports on surface modification of C_{60} [31] and their utilization as nanofiller in epoxy restrict us to make out a broad conclusion. This led the foundation to investigate the effect of oxidation and silanization of C_{60} on properties of epoxy nanocomposites. A detailed investigation on micro-scale properties such as morphological, physical nature, defect density and thermal degradation behavior of stepwise modified C_{60} has been performed. The aim of the work was achieved by analyzing the micro-scale properties such as molecular architecture and defect density due to oxidation and silanization of oxidized and silanized C_{60} and interlinking them with the meso-scale properties of C_{60}/epoxy determined from dynamic-mechanical analysis and thermogravimetric analysis. We believe that enhanced defect density after oxidation generates more sites for silanization, which subsequently affects the molecular interaction of C_{60} with the epoxy network and thus tailors the dynamic-mechanical performance of epoxy nanocomposites.

2. Experimental

2.1. Oxidation and silanization of fullerene

In the present work, fullerenes, C_{60} (P-Fs), (99%, NanoShell, USA) of average diameter 60–80 nm were stepwise modified according to the reaction mechanism schematically illustrated in Fig. 1. Oxidation of the P-Fs was done in presence of concentrated nitric acid, HNO_3 0.3 g of P-Fs in 20 ml of conc. HNO_3 (69%, Merck) under continuous mechanical stirring at 600 rpm and at constant temperature of 80 °C for 1.5 h. Later the solution was washed and filtered using double distilled water, ethanol and acetone in sequence until pH 7 is reached. The oxidized fullerenes (O-Fs) is obtained after drying in oven at 80 °C for 8 h. The oxidation derivative of P-Fs is demonstrated by reaction 1 as shown in Fig. 1.

The possible reaction mechanism of forming oxygenated functional elemental group onto P-Fs during acidic reaction involves two steps. In the first step, NO_2^+ (from HNO_3) was hypothetically added to the olefin moieties of the C_{60} through electrophilic reaction forming C=C bond with P-Fs. In the second step, this addition of NO_2^+ is substituted with water to introduce the oxygenated functional elemental group by nucleophilic reaction. The evidence of forming such functional group under acidic condition is also reported by others [40,41]. For the preparation of APTES-derived silane layer [42] and to prevent the loss of the APTES functional elements during the silanization process [43,44], O-Fs were dispersed and mixed in toluene (0.3 g of O-Fs in 25 ml of toluene) and bath sonicated for 1 h in a round bottom flask. While doing the bath sonication, mixture of 5 ml toluene with 3-aminopropyltriethoxysilane (APTES, 99% Alfa Aesar, India) (1 wt% of O-Fs) was added drop wise to the above solution. The obtained resultant reaction mixture, as illustrated by reaction 2 in Fig. 1, was refluxed at constant temperature of 110 °C and simultaneously stirred for 8 h at 600 rpm. The refluxed solution was filtered and washed several times with double distilled water, ethanol and acetone in sequence. The final product in the form of silanized fullerenes (S-Fs) was obtained after oven drying at 80 °C for 8 h. APTES functional elements are covalently attached with the oxygenated functional elemental group of O-Fs during the silanization process to form siloxane layer onto the surfaces of O-Fs as demonstrated schematically by reaction 2 in Fig. 1.

2.2. Preparation of C_{60}/epoxy nanocomposites

The C_{60}/epoxy nanocomposites were prepared using stepwise modified C_{60} and epoxy network consisting of Diglycidylether of bisphenol-A resin (Lapox-L12) and Triethylenetetramine hardener (TETA-K6) (Atul, India). In a particular processing, P-Fs (0.5 wt %) were blended in epoxy resin using an ultrasonic processor (Q700, Qsonica, USA) at an amplitude of 70% for 1 h. To overcome the temperature rise above 40 °C, processing was done in pulsation mode under the circulation of chilled water. Later curing agent was added with a proportion of 12:1 by weight and mechanically mixed for 10 min at room temperature. The P-Fs epoxy nanocomposite (P-FEC) is obtained by degassing (for removal of entrapped air) followed by curing at 80 °C for 2 h. Similar process is followed for preparation of O-Fs and S-Fs epoxy nanocomposite (O-FEC and S-FEC). The neat epoxy (NE) composite was prepared following the same processing route but without C_{60}. The possible reaction mechanism of S-Fs with epoxy network is demonstrated schematically in Fig. 2.

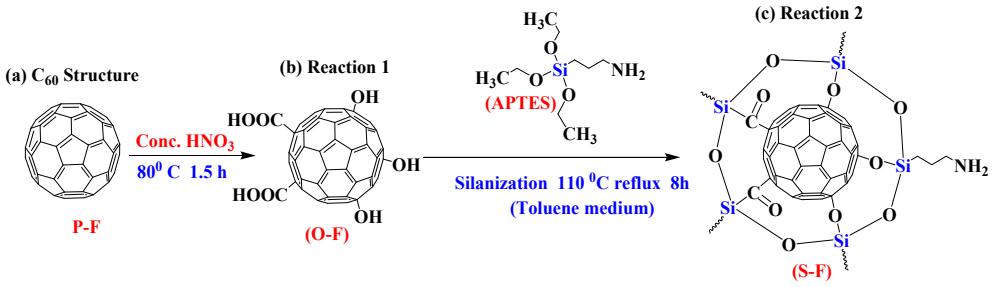

Fig. 1. Schematic representation of C_{60} stepwise modification.

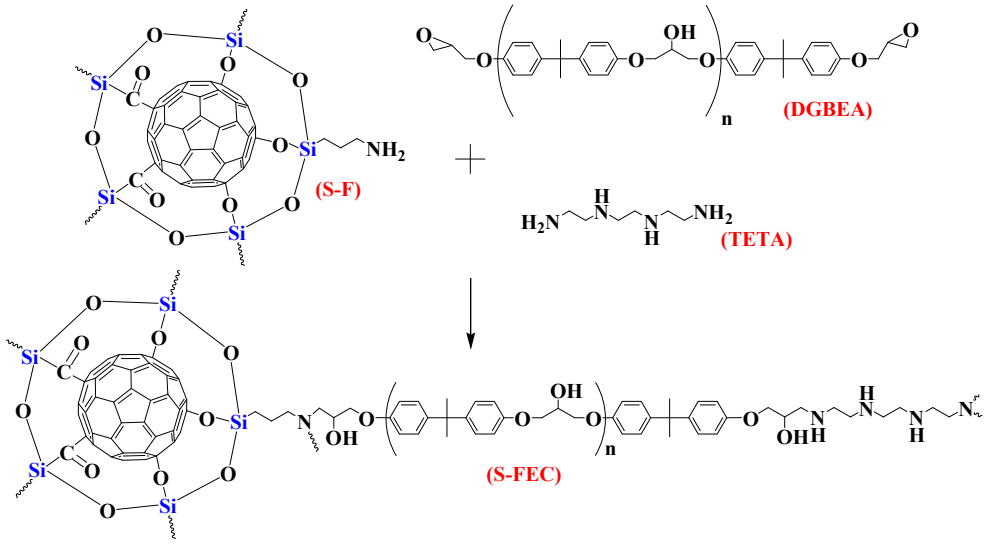

Fig. 2. Curing mechanism of S-F with epoxy resin.

2.3. Characterization

Microscopy at high resolution was performed under field emission scanning electron microscope (FESEM, Zeiss, Supra 55VP microscope) at an acceleration voltage of 5 kV. Transmission electron microscopy (TEM) of C_{60} is performed on JEM-2100 HRTEM, JEOL, Japan, operated at 200 kV. The C_{60} was dispersed in ethanol using ultrasonification for 30 min and the obtained suspension is placed on copper grid. The infrared spectra of C_{60} was recorded from 400 to 4000 cm^{-1} with resolution of 0.2 cm^{-1} under Fourier transformed infrared spectroscopy (FTIR- Bruker Vertex 80 spectrometer, Germany). The FT-RAMAN spectra of P-Fs, O-Fs and S-Fs, were recorded under Bruker RFS 27: Standalone FT-Raman spectrometer, resolution of 2 cm^{-1} using an Nd: YAG laser source at 1064 nm wavelength. The signature of thermo mechanical behavior for NE, P-FEC, O-FEC and S-FEC were obtained from dynamic mechanical analyzer (DMA 8000 PerkinElmer system, U.S.A). The tests were carried out under single cantilever mode for specimens with dimension of 25 × 8 × 2 mm^3 at an oscillation frequency of 1 Hz. Data were collected from room temperature to 120 °C at a scanning rate of 2 °C/min. Thermogravimetric analysis (TGA) was recorded from a thermal analyzer, NETZSCH STA 449F3 system, Germany. The test was carried out at a heating rate of 10 °C/min from room temperature to 700 °C under nitrogen purging gas with flow rate of 200 ml/min using alumina as the reference material.

3. Results and discussions

3.1. Morphological analysis

The most obvious evidence enlightening the stepwise modification of C_{60} can be demonstrated through the dispersion analysis. Fig. 3 shows that P-Fs sediments completely after 24 h of sonication whereas, the O-Fs and S-Fs remained colloidal (well dispersed) in DMF. However, no change in the colloidal state of O-Fs and S-Fs in

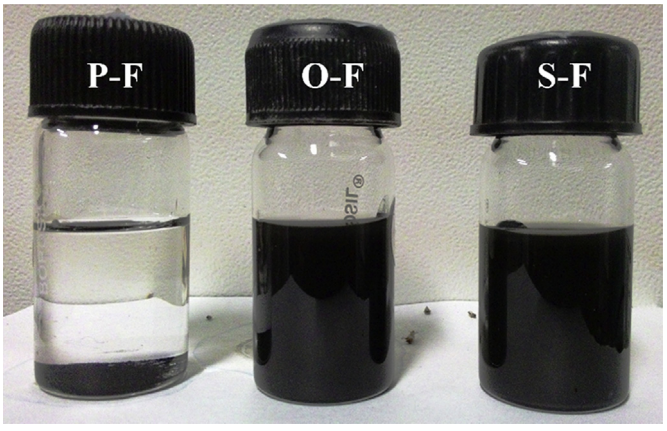

Fig. 3. Colloidal dispersion of P-F, O-F and S-F in DMF.

DMF is found even after 25 days. This well dispersed nature for O-Fs and S-Fs is possibly owing to the formation of equally charged functional groups onto P-Fs as reported for CNTs [38,45]. Long term colloidal stability is primarily due to the steric hindrance caused by the similar charged particles present on the surfaces of modified fullerenes resulting in repulsion amongst them.

Morphological investigation of P-Fs, O-Fs and S-Fs under FESEM, as can be seen in Fig. 4, reveals presence of similar spherical morphology of O-Fs and S-Fs akin to that of the P-Fs. But, highly interconnected networks of C_{60} irrespective of oxidation and silanization is observed from FESEM investigation. However, high magnification FESEM investigation (shown in top right corner of Fig. 4(a–c)) reveals irregular and non-uniform surfaces of O-Fs (Fig. 4(b)) and S-Fs (Fig. 4(c)) when compared to P-Fs (Fig. 4(a)). The variation of carbon and oxygen content for P-Fs, O-Fs and S-Fs is subsequently studied under EDX and illustrated in Fig. 4(d). It is found that for P-Fs, O-Fs and S-Fs, carbon content is 83.34, 81.22 and 77.31 wt% and oxygen content is 6.31, 8.41 and 10.92 wt %. Decrease in carbon content for O-Fs and S-Fs indicates possibility of removing strong disordered structure of amorphous carbon due to HNO_3 treatment that might be existing in P-Fs. On the other hand, increase in oxygen content for O-Fs and S-Fs is predictive for attachment of oxygenated functional elemental groups [46]. In case of S-Fs, increase in oxygen content and generation of new deceptive peak of Si at 1.7 keV indicates covalent attachment of siloxane group through the possible reaction mechanism schematically demonstrated in Fig. 1.

Further validation of the morphological structure of silanized C_{60} is obtained from TEM investigation as shown in Fig. 5. Morphology of S-Fs under TEM, again confirms their tightly inter connected network (Fig. 5(a)). This is possibly because of reverse attachment of APTES onto the defect sites of O-Fs. A layer of APTES grafting onto C_{60} surface is evident from the TEM image as shown in Fig. 5(b). Investigation at higher magnification under TEM demonstrates better visibility of that layer sized ~2.5 nm (shown in insert top right corner of Fig. 5(b)). Thus, in brief stepwise modification of fullerenes preserves the power to form layered structure onto their surfaces which, are expected to interact with epoxy network to tailor the composite properties.

3.2. FTIR spectroscopic analysis

The similarity and differences in molecular architecture due to stepwise modification of C_{60} were corroborated from FTIR, and the normalized spectroscopic results are shown in Fig. 5. Intense common peaks of pristine and modified C_{60} at frequencies 580, 1183 and 1437 cm^{-1} are observed (enlarged view in Fig. 6). However, there was variation in intensities of these vibration bands for O-Fs and S-Fs, suggesting decreased interaction amongst C_{60} [47]. Pristine and modified C_{60} showed presence of (-OH) group at frequency 3440 cm^{-1} arising from adsorbed atmospheric moisture [30]. Intensity of the (-OH) group peak is found decreased after oxidation and silanization. Reduced symmetric and asymmetric stretching (2926 cm^{-1} and 2855 cm^{-1}) of CH_2 group is also observed due to modification [48,49]. The evidence of (-COOH) group formation is demonstrated through the new peak generated for O-Fs (1726 cm^{-1} and 1223 cm^{-1}) corresponding to the C=O and C–O stretching [16,22]. Further confirmation is drawn through the presence of new bands at 1620 cm^{-1} and 1380 cm^{-1}, arising from intermediate oxidation products [50] and O–H bending vibration [51]. The difference in spectra's for S-Fs mainly arises from the disappearance and appearance of various peaks in comparison to P-Fs and O-Fs. One such example was harvested from the appearance of peak at 1595 cm^{-1} (primary NH_2 of APTES) and disappearance of

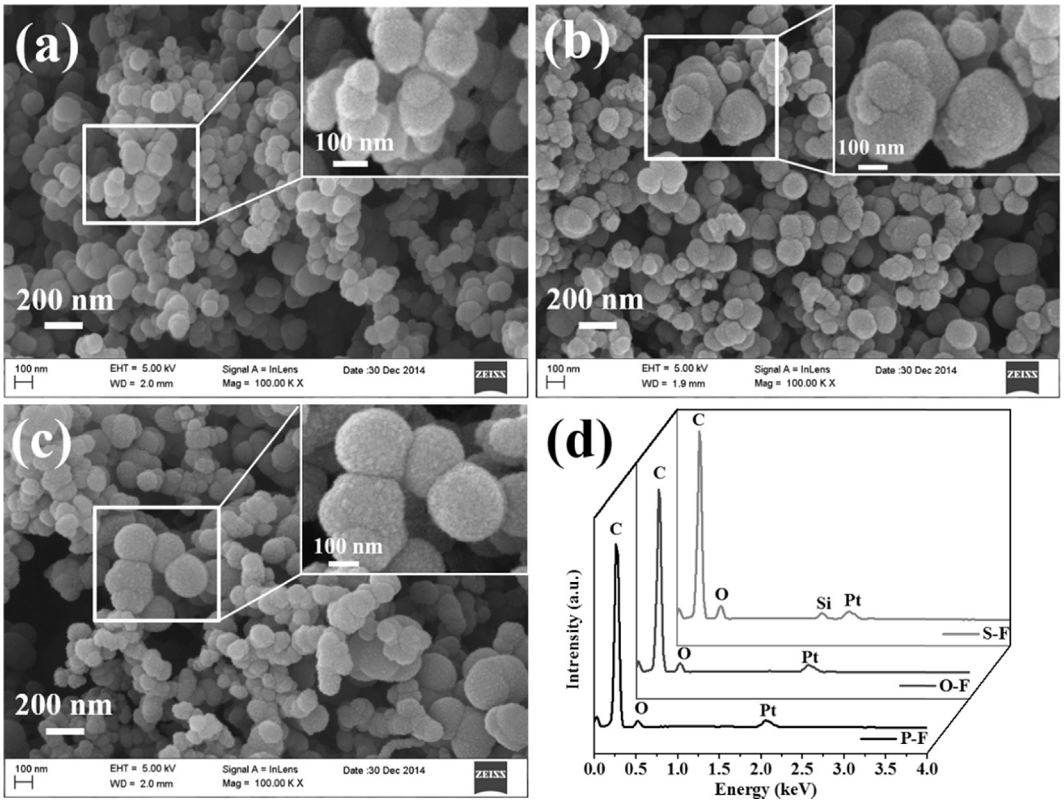

Fig. 4. Representative FESEM images of (a) P-F, (b) O-F and (c) S-F as well as (d) EDX analysis of pristine and stepwise modified C_{60}.

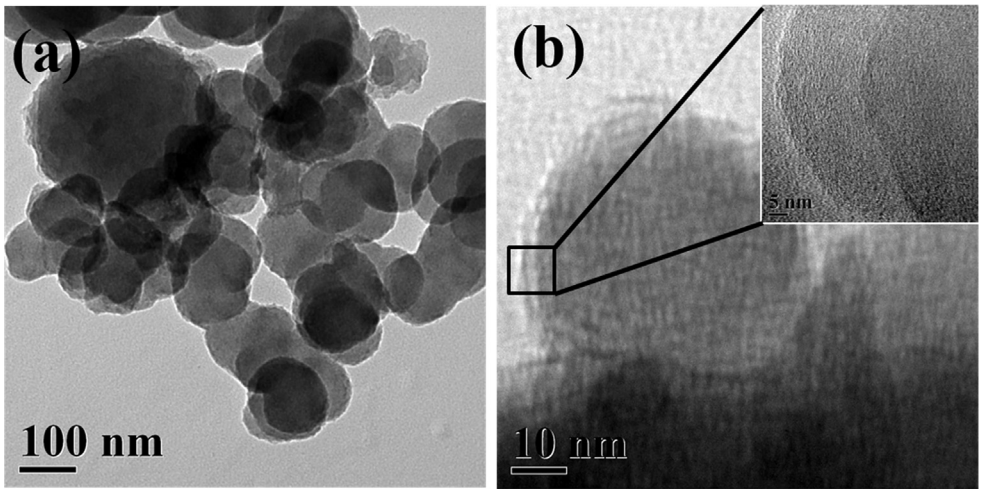

Fig. 5. Representative TEM micrograph of S-F (a) low magnification and (b) high magnification.

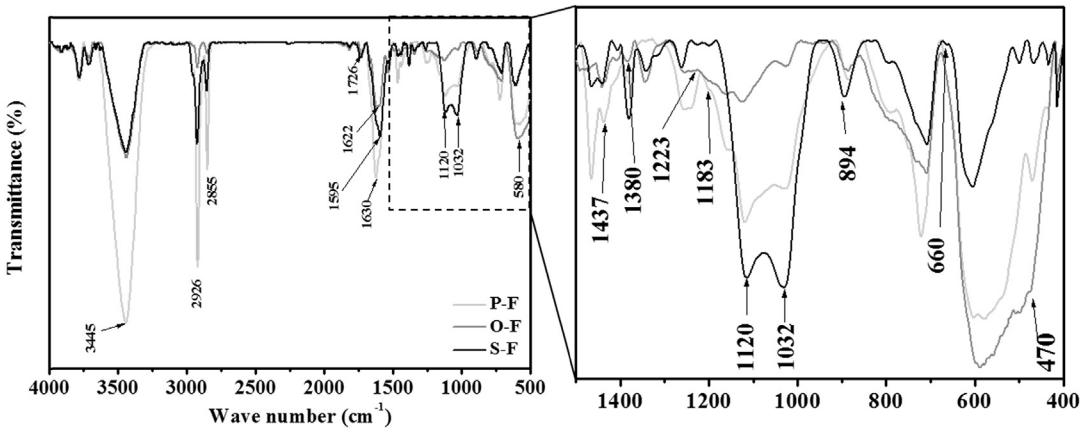

Fig. 6. Normalize FTIR spectra of P-F, O-F and S-F.

peak at 1622 cm^{-1} (C=C stretching) [52]. Appearance of additional bands conjugated at frequencies 1120 cm^{-1} and 1032 cm^{-1} (Si–O–Si stretching) [34,52], 660 cm^{-1} (Si–C), 894 cm^{-1} (hydrolyzed silane, Si–OH) is found. This confirms the attachment of the siloxane group along with hydrophilic NH_2 onto C_{60}.

3.3. TGA analysis

The Surface modification of C_{60} was also evident under TGA and DTG analysis as shown in Fig. 7. The pristine and the stepwise modified C_{60} shows ~2% weight loss from the TGA curves within the temperature range of 35–150 °C primarily arising from the evaporation of absorbed moisture from their surfaces. The signature of such degradation is predictive from the peak generated in the DTG curves within that temperature range. In case of P-Fs, no further distinguishable DTG peaks were observed corresponding to the TGA weight loss behavior. But, for O-Fs and S-Fs, DTG peak corresponding to ~5% weight loss within temperature range of 150–300 °C is observed, primarily elucidating the degradation of surface functional elemental groups [53]. However, no additional DTG peaks for O-Fs is observed corresponding to TGA weight loss with increase in temperature. But, in comparison to O-Fs the DTG profile of S-Fs demonstrates a new deceptive peak generated and is corresponding to ~7% weight loss (from TGA curve) within the temperature range of 300–450 °C. This peak is predictive for APTES

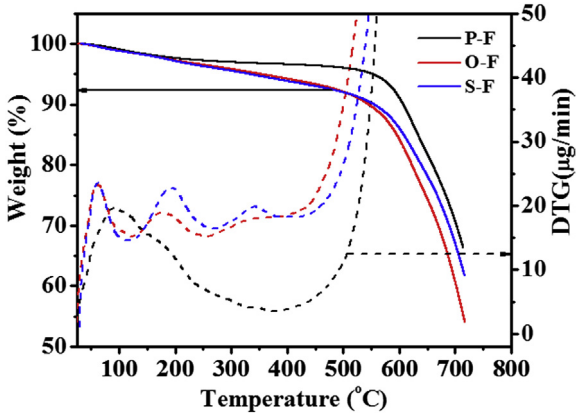

Fig. 7. Normalize TGA and DTG profile of P-F, O-F and S-F.

functional group degradation from the surfaces of S-Fs. Moreover, the weight residue at 700 °C of O-Fs (~61 wt%) is found lesser than that of P-Fs (~71 wt%). Acid treatment of P-Fs might have reduced the amount of impurities and amorphous carbon and thus resulted in lowering of the residual weight fraction. However, for S-Fs a slight increment in weight residue fraction (~67 wt%) compared to

that of O-Fs is found might be because of the presence of Si group from the APTES functional elements.

3.4. Raman spectroscopic analysis

The effect of oxidation and silanization on defect density of C_{60} during stepwise modification is investigated under Raman spectroscopy. The investigation highlights the differences in the degree of structural ordering and bonding states of C_{60} due to stepwise modification as depicted in Fig. 8. Two major characteristic peaks of P-Fs near 1479 cm^{-1} and 1532 cm^{-1} was observed, corresponding to the A_g bands from pentagonal pinching [3,54]. This is mainly arising from the vibration of 5-member rings and ring deformation of 6-membered rings [55]. Such bands predicts purity of the samples, even though disordered structure of amorphous carbon is evident from strong band at 1300 cm^{-1}. Additional bands in the spectra of P-Fs at 1364 cm^{-1} (D-band) and 1590 cm^{-1} (G-band) is observed. D-band is mainly ascribed to the presence of disordered carbon in fullerene [38]. On the other hand, G-band represents crystalline graphitic structures [55]. Significant reduction in these band intensities has been observed after oxidation, possibly owing to removal of amorphous carbon during oxidation, represented through broadening of peak at 1319 cm^{-1}. Additionally, upshifting of Raman wave number associated with G-band was observed (Fig. 8), might be owing to the complexation power of C_{60} which may be arising due to electron accepting capability of P-Fs [54]. Substantial effect after silanization is depicted through significant reduction of intensity and downshift of D-band and G-band for S-Fs. This downshift results in Raman vibration band at 1290 cm^{-1} and 1590 cm^{-1} for D-band and G-band respectively. Attachment of APTES functional elemental group onto O-Fs might have reduced the complexation power of C_{60} thereby, resulting in down shift of the resonance. The intensity ratio between D-band and G-band (I_G/I_D) is used to determine defect density [3,51,56]. The I_G/I_D ratio enhances to 10% (0.97 (O-Fs) from 0.88 (P-Fs)) after oxidation, while the enhancement is 20.5% (1.06 (S-Fs)) for S-Fs when compared to P-Fs. An increase in I_G/I_D ratio indicates an increment in the number of defect sites.

3.5. Dynamic-mechanical properties of C_{60}/epoxy nanocomposites

The variation in relaxation behavior of the C_{60}/epoxy nanocomposites under load and temperature was ascertained under DMA as can be seen in Fig. 9. The storage modulus, G' (MPa) and damping factor, tan δ, variation with temperature for NE as well as P-FEC, O-FEC and S-FEC is depicted in Fig. 9(a) and (b) respectively. The storage modulus curves endorses valuable insight predicting the stiffness and molecular relaxation in NE and C_{60}/epoxy nanocomposites. Fig. 9(a) evidences the significant variation of the G' of epoxy nanocomposites with pristine and stepwise modified C_{60} with respect to NE. At room temperature the G' for NE is ~148 MPa, which has been enhanced to values ~605, ~592 and ~875 MPa for P-FEC, O-FEC and S-FEC. Hence, demonstrating a significant enhancement of G' by ~308%, ~300% and ~491% for P-FEC, O-FEC and S-FEC with respect to NE. However, marginal variation in modulus in case of O-FEC is observed in comparison to P-FEC. Thus, attachment of oxygenated functional elemental group onto C_{60} surfaces provides no such appreciable effect to enhance G' within the glassy region of epoxy nanocomposite [27,57]. This fact may be attributed to the formation of plasticizing mobile phase around C_{60} surfaces due to the presence of oxygenated functional groups, leading to de-bonded aggregates which are weekly bonded to epoxy. In other words, with increase in temperature homopolymerization or esterification reaction adjacent to the phases near C_{60} facilitates modulus degradation as evident from narrowing the temperature window for O-FEC, as can be seen in Fig. 9(a). On the other hand, broadening of the temperature window corresponding to G' degradation is achieved for S-FEC. This behavior predicts the formation of high modulus interfaces between S-Fs and epoxy. Thus, the significant improvement of G' for S-FEC is mainly owing to the silanization effect.

Further understanding of the mobility of the epoxide group due to stepwise modification of C_{60} is done through the investigation of damping factor behavior (position and intensity), tan δ, representing the glass transition temperature (T_g) as shown in Fig. 9(b). The T_g of the epoxy composites at a specific temperature can be related to Brownian motion of the main chains [58]. The addition of P-Fs, O-Fs and S-Fs in epoxy resin leads to progressive decrease in T_g but, increases the intensity of tan δ peak. The damping factor intensity enhancement is mainly associated with material ability to dissipate higher energy through segmental motion [33,58]. The S-FEC showed enhanced intensity of tan δ peak, attributed to high energy absorption during viscoelastic motion. In general, the decrease in T_g of epoxy nanocomposites is associated with improper curing stoichiometry between epoxy and hardener due to addition of nanofillers, the same is also reported in other refs. [59–61]. The incorporation of different functional groups onto the carbon nanofiller results in steric and reactivity differences, which may restricts the cross-linking process of the epoxy network during curing, leading to change in T_g [62]. The depression in T_g for S-FEC might be because of alteration in curing stoichiometry and therefore subsequently decreases the cross-link density. Moreover, the formation of siloxane group onto C_{60} results in excess amine group formation, which possibly be the reason to alter the T_g [61]. To endorse this phenomenon interfacial interaction between the C_{60} and the epoxy matrix was investigated by using the correlation between damping factor of the C_{60}/epoxy nanocomposites and neat epoxy utilizing the equation shown below [63].

$$\tan\delta = \tan\delta_m/(1 + B\varphi) \quad (1)$$

Where tanδ and tanδ_m are the loss tangent of the C_{60}/epoxy nanocomposite and neat epoxy, respectively, φ represents the volume fraction of the nanofillers and B is an interaction parameter which is a quantitative measurements of interfacial interaction between the nanofillers and the epoxy network. A larger value of B means a better interaction between the two phases. From Fig. 9(b) it is observed that the peak value of tanδ of the P-FEC (1.34) is higher than that of the NE (0.89), and the interaction parameter ($B = -0.61$) is low and negative, which indicates a relatively weak

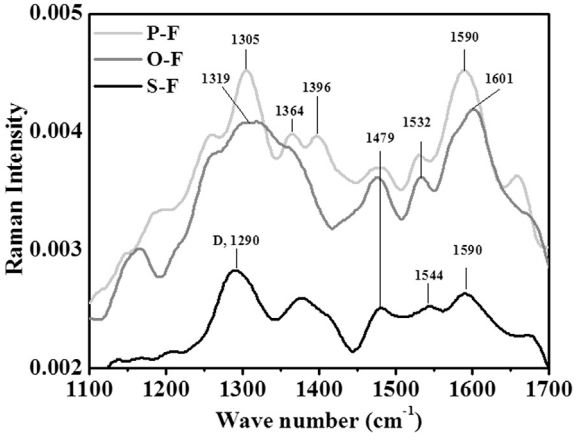

Fig. 8. Normalize Raman spectra of P-F, O-F and S-F.

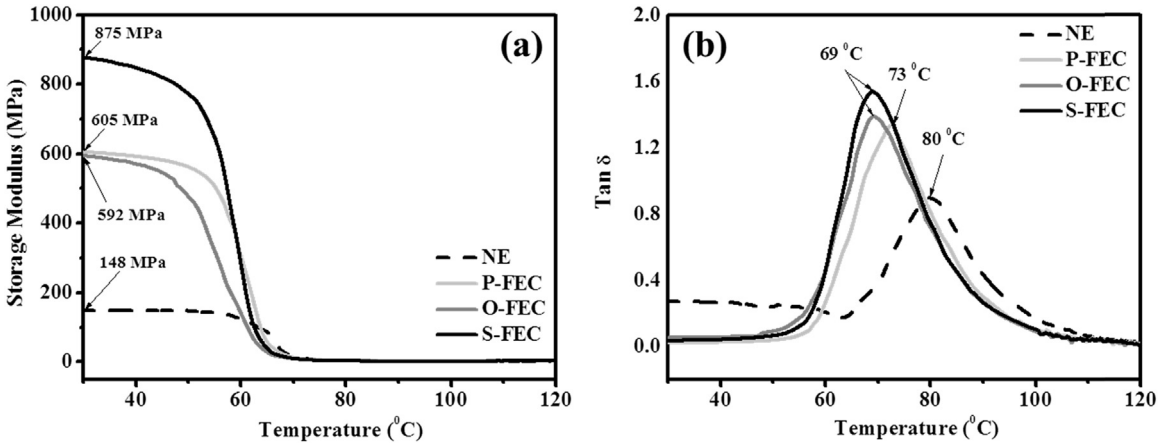

Fig. 9. DMA results for NE as well as pristine and modified C_{60}/epoxy nanocomposites: (a) storage modulus-temperature curves; (b) loss factor (tan δ)-temperature curves.

physical interaction between the P-Fs and epoxy network. The peak values of tanδ for O-FEC (1.39) and S-FEC (1.54) is also higher than that of P-FEC and NE. The interaction parameter for O-FEC and S-FEC is calculated as −0.65 and −0.77 respectively, indicating weak physical interaction for O-FEC and S-FEC. In general, a complex interaction dominates the properties of nanofiller incorporated in epoxy composites. Moreover, the interaction behavior vary greatly for different matrix-filler systems. In case of step-wise modified C_{60}, presence of oxygenated and siloxane functional group makes the interaction phenomenon further complicated. The plasticizing mobile phase around C_{60} surfaces due to the presence of functional groups elements might be leading to de-bonded aggregates at elevated temperature making them weekly bonded to the epoxy. Furthermore, the height and breadth of the tanδ peaks provides additional information about the molecular relaxation of the samples. The interfacial load transfer between C_{60} and epoxy network can be understood form the tanδ peak intensity, where low intensity is a measure of efficient stress transfer and large intensity indicates relatively viscous response to stress at epoxy-nanofiller interface during glass transition [28,62,64]. The significant decrease in breath of the peak for the C_{60}/epoxy nanocomposite suggest a narrower distribution of relaxation times, presumably due to enhanced Brownian motion of the main chains and less interaction between C_{60} and epoxy network as indicated by B and hence influences the mobility of epoxy network at T_g [65]. At the temperature, near T_g no significant variation in G' is observed for pristine and stepwise modified C_{60}/epoxy nanocomposites, which indicates loose interaction and relatively high viscous flow. Moreover, the presence of flexible Si−O−Si bonds at the interfaces between C_{60} and epoxy network as shown in Fig. 2, possibly reduces the interaction [28].

3.6. Thermogravimetric analysis of C_{60}/epoxy nanocomposites

The effect of oxidation and silanization on the thermal stability of P-FEC, O-FEC and S-FEC were investigated under TGA, and shown in Fig. 10. The T_{IDT} (5% weight loss), T_{MDT} (50% weight loss) and CY% of the NE and epoxy nanocomposite are obtained from the representative TGA thermogram of P-FEC, O-FEC and S-FEC (Fig. 10(a)). The variation in IDT, MDT and CY% for NE, P-FEC, O-FEC and S-FEC is shown in Fig. 10(b). The TGA thermogram clearly evidences single decomposition stage for NE as well as C_{60}/epoxy nanocomposites. In case of P-FEC, T_{IDT} value (333 ± 5.9 °C) is higher than NE (321 ± 6.32 °C). But the T_{IDT} for O-FEC is 28 °C lower than NE. Incorporation of S-Fs in epoxy resulted in modest increase of T_{IDT} value. Similar behavior is evident in case of T_{MDT}. It can be observed that, T_{MDT} is unaltered for P-FEC (389 ± 6.3 °C) with respect to NE. A modest reduction in T_{MDT} by 5 °C is evident for O-FEC but, after incorporation of S-Fs in epoxy T_{MDT} becomes equal to that of the NE. In case of P-FEC, inherent capability of P-Fs to form non-covalent donor-acceptor compound with epoxy, inhibits radical and branched chain reaction [14,66] thereby, restricts molecular mobility of polymer chain. Thus, delays the predominant random chain scission of the epoxy matrix during the initial step of thermal degradation [67]. At high temperature above 300 °C, P-Fs is having high efficacy to degrade through intensive oxidation and thus, exerts their stabilization power. This results in rupture of weak bond between polymer and C_{60}. The negative effect on thermal stability of O-FEC is owing to the oxygenated functional elemental group attachment onto C_{60} making them probably incapable to react with radicals of different chemical nature in epoxy. Moreover, oxidized C_{60} in epoxy possibly catalyzes rupture of weak bond leading to decreased structural stability. But, in case of S-FEC existence of siloxane along with NH_2 hydrophilic group onto C_{60} enhances the strong chemical interaction between the epoxy matrix and S-Fs through the interfaces. This is leading to increased T_{IDT} as well as T_{MDT} for S-FEC compared to O-FEC by restricting the molecular mobility of the polymer chain during initial degradation and restricting rupture of weak bond at high temperature. The CY% illustrates the change in the weight % of NE and C_{60}/epoxy nanocomposites at 700 °C. The CY% for P-Fs was higher mainly due to partial decomposition at 700 °C in comparison to other modified epoxy nanocomposites. The reduction in CY% for O-FEC suggest, enhanced thermal degradation of O-Fs. The marginal increase in CY % for S-FEC predicts strong interfacial chemical interaction through the interfaces formed due to siloxane and NH_2 hydrophilic group. Taking in account the thermal degradation behavior, it can be established that pristine as well as silanized C_{60} play better stabilizing role to enhance thermal stability of epoxy nanocomposites.

4. Conclusion

We have exposed the dynamic mechanical properties and thermal stability of stepwise modified C_{60}/epoxy nanocomposite. The modification is done through oxidation and silanization in presence of APTES to attach siloxane group onto C_{60}. Dispersion behavior under DMF demonstrates the formation of colloidal suspension for O-Fs and S-Fs indicating better dispersion. FESEM investigation revealed similar spherical morphology of O-Fs and S-Fs akin to that of the P-Fs. But, O-Fs and S-Fs remained highly

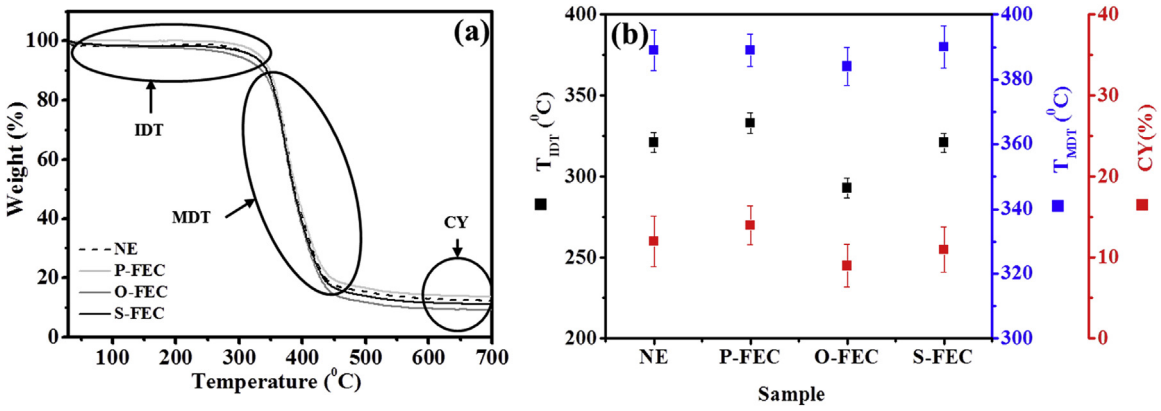

Fig. 10. Representative (a) TGA curves of NE, P-FEC, O-FEC and S-FEC and (b) T_{IDT} (5% weight loss), T_{MDT} (50% weight loss) and CY% of NE and C_{60}/epoxy nanocomposites.

interconnected even after surface modification. The presence of Si with decreased carbon and increased oxygen content is evident from EDX analysis of S-Fs. A careful investigation of S-Fs under TEM reveals the formation of siloxane layer (~2.5 nm). The spectroscopic studies conducted under FTIR and TGA-DTG analysis confirms successful oxidation and silanization of C_{60}. Raman spectroscopy endorses reduced interaction amongst C_{60} for S-Fs but, confirms presence of some structural defects even after silanization. In accord with the DMA results, room temperature storage modulus was enhanced by ~491% for S-FEC. This is attributed to the enhanced stiffness and molecular relaxation by improved interfacial adhesion, which, compensates the plasticizing effect around the interphase of C_{60}. However, covalent attachment of the oxygenated functional elemental group onto C_{60} apparently showed no such appreciable potentiality to enhance storage modulus within the glassy region. The addition of S-Fs in epoxy resin resulted decreased T_g, but, tan δ peak intensity was increased. On the other hand, the thermal stability of the epoxy nanocomposite system was not affected due to addition of S-Fs. These observations clearly demonstrates the potential effectiveness of silanized C_{60} as a reinforcement for epoxy nanocomposites to improve the viscoelastic and thermal performance.

Acknowledgment

The authors thanks Department of Science and Technology, India under DST-FIST program 2014 with Grant No. SR/FST/ETI-373/2014. This work was initiated under the project head “Synthesis and Fracture Property Evaluation of Polymer Nano composites” supported by National Institute of Technology Silchar, Assam, India (Project number (RC)/457/122). Author is also acknowledging SAIF-IIT Bombay, SAIF-IIT Madras and IIT Roorkee for FT-IR, FT-RAMAN and DMA analysis.

References

[1] F. Pervin, Y. Zhou, V.K. Rangari, S. Jeelani, Testing and evaluation on the thermal and mechanical properties of carbon nano fiber reinforced SC-15 epoxy, Mater Sci. Eng. A 405 (2005) 246–253, http://dx.doi.org/10.1016/j.msea.2005.06.012.

[2] L. Sacarescu, S. Kostromin, S. Bronnikov, Synthesis and properties of polydiphenylsilane/fullerene C_{60} nanocomposites, Mater Chem. Phys. 149–150 (2015) 430–436, http://dx.doi.org/10.1016/j.matchemphys.2014.10.041.

[3] T. Soga, T. Kondoh, N. Kishi, Y. Hayashi, Photovoltaic properties of an amorphous carbon/fullerene junction, Carbon 60 (2013) 1–4, http://dx.doi.org/10.1016/j.carbon.2013.02.050.

[4] K. Song, Y. Zhang, J. Meng, E.C. Green, N. Tajaddod, H. Li, et al., Structural polymer-based carbon nanotube composite fibers: understanding the processing-structure-performance relationship, Materials 6 (2013) 2543–2577, http://dx.doi.org/10.3390/ma6062543.

[5] T. Kashiwagi, E. Grulke, Thermal degradation and flammability properties of poly (propylene)/carbon nanotube composites, Macromol. Rapid Commun. 23 (2002) 761–765, http://dx.doi.org/10.1002/1521-3927(20020901)23:13<761::AID-MARC761>3.0.CO;2-K.

[6] Y. Liu, S. Kumar, Polymer/carbon nanotube nano composite fibers-a review, ACS Appl. Mater Interfaces 6 (2014) 6069–6087, http://dx.doi.org/10.1021/am405136s.

[7] M.S. Goyat, S. Suresh, S. Bahl, S. Halder, P.K. Ghosh, Thermomechanical response and toughening mechanisms of a carbon nano bead reinforced epoxy composite, Mater Chem. Phys. 166 (2015) 144–152, http://dx.doi.org/10.1016/j.matchemphys.2015.09.038.

[8] M.A. Rafiee, J. Rafiee, I. Srivastava, Z. Wang, H. Song, Z.Z. Yu, et al., Fracture and fatigue in graphene nanocomposites, Small 6 (2010) 179–183, http://dx.doi.org/10.1002/smll.200901480.

[9] K. Lau, M. Lu, H. Cheung, F. Sheng, H. Li, Thermal and mechanical properties of single-walled carbon nanotube bundle-reinforced epoxy nanocomposites: the role of solvent for nanotube dispersion, Compos Sci. Technol. 65 (2005) 719–725, http://dx.doi.org/10.1016/j.compscitech.2004.10.005.

[10] L. Guadagno, L. Vertuccio, A. Sorrentino, M. Raimondo, C. Naddeo, V. Vittoria, et al., Mechanical and barrier properties of epoxy resin filled with multiwalled carbon nanotubes, Carbon 47 (2009) 2419–2430, http://dx.doi.org/10.1016/j.carbon.2009.04.035.

[11] V. Leon, R. Parret, R. Almairac, L. Alvarez, M.-R. Babaa, B.P. Doyle, et al., Spectroscopic study of double-walled carbon nanotube functionalization for preparation of carbon nanotube/epoxy composites, Carbon 50 (2012) 4987–4994, http://dx.doi.org/10.1016/j.carbon.2012.06.007.

[12] E. Badamshina, M. Gafurova, Polymeric nanocomposites containing non-covalently bonded fullerene C60: properties and applications, J. Mater Chem. 22 (2012) 9427–9438, http://dx.doi.org/10.1039/c2jm15472b.

[13] P.A. Troshin, O.A. Mukhacheva, Ö. Usluer, A.E. Goryachev, A.V. Akkuratov, D.K. Susarova, et al., Improved photovoltaic performance of PPV-based copolymers using optimized fullerene-based counterparts, Adv. Energy Mater 3 (2013) 161–166, http://dx.doi.org/10.1002/aenm.201200118.

[14] L. Zhao, Z. Guo, Z. Cao, T. Zhang, Z. Fang, M. Peng, Thermal and thermo-oxidative degradation of high density polyethylene/fullerene composites, Polym. Degrad. Stab. 98 (2013) 1953–1962, http://dx.doi.org/10.1016/j.polymdegradstab.2013.07.020.

[15] I. Montanari, A.F. Nogueira, J. Nelson, J.R. Durrant, C. Winder, M.A. Loi, et al., Transient optical studies of charge recombination dynamics in a polymer/fullerene composite at room temperature, Appl. Phys. Lett. 81 (2002) 3001–3003, http://dx.doi.org/10.1063/1.1512943.

[16] M.A. Rafiee, F. Yavari, J. Rafiee, N. Koratkar, Fullerene–epoxy nanocomposites-enhanced mechanical properties at low nanofiller loading, J. Nanopart Res. (2011) 733–737, http://dx.doi.org/10.1007/s11051-010-0073-5.

[17] L. Zhao, P. Song, Z. Cao, Z. Fang, Z. Guo, Thermal stability and rheological behaviors of high-density polyethylene/fullerene nanocomposites, J. Nanomater 2012 (2012) 1–6, http://dx.doi.org/10.1155/2012/340962.

[18] T. Ogasawara, Y. Ishida, T. Kasai, Mechanical properties of carbon fiber/fullerene-dispersed epoxy composites, Compos Sci. Technol. 69 (2009) 2002–2007, http://dx.doi.org/10.1016/j.compscitech.2009.05.003.

[19] S. Halder, P.K. Ghosh, M.S. Goyat, Influence of ultrasonic dual mode mixing on morphology and mechanical properties of ZrO_2-epoxy nanocomposite, High. Perform. Polym. 24 (2012) 331–341, http://dx.doi.org/10.1177/0954008312440714.

[20] S. Halder, M. Goyat, P. Ghosh, Morphological, structural, and thermophysical properties of zirconium dioxide-epoxy nanocomposites, High. Perform. Polym. (2015), http://dx.doi.org/10.1177/0954008315595275.

[21] E.B. Zeinalov, G. Koßmehl, Fullerene C_{60} as an antioxidant for polymers, Polym. Degrad. Stab. 71 (2001) 197–202, http://dx.doi.org/10.1016/S0141-3910(00)00109-9.

[22] Y. Sun, H. Bao, M. Jia, Z. Guo, J. Yu, Effect of the silanization processes on the

properties of oxidized multiwalled carbon nanotubes, Acta Phys. Pol. A 116 (2009) 150–155, http://dx.doi.org/10.3724/SP.J.1105.2009.00684.
[23] C. Velasco-Santos, A.L. Martinez-Hernandez, W. Brostow, V.M. Castaño, Influence of silanization treatment on thermomechanical properties of multiwalled carbon nanotubes: poly(methylmethacrylate) nanocomposites, J. Nanomater 2011 (2011) 1–9, http://dx.doi.org/10.1155/2011/928659.
[24] J. Zhu, S. Wei, J. Ryu, M. Budhathoki, G. Liang, Z. Guo, In situ stabilized carbon nanofiber (CNF) reinforced epoxy nanocomposites, J. Mater Chem. 20 (2010) 4937–4948, http://dx.doi.org/10.1039/c0jm00063a.
[25] Y. Nie, T. Hübert, Surface modification of carbon nanofibers by glycidoxysilane for altering the conductive and mechanical properties of epoxy composites, Compos Part A 43 (2012) 1357–1364, http://dx.doi.org/10.1016/j.compositesa.2012.03.025.
[26] M. Naebe, J. Wang, A. Amini, H. Khayyam, N. Hameed, L.H. Li, et al., Mechanical property and structure of covalent functionalised graphene/epoxy nanocomposites, Sci. Rep. 4 (2014) 1–7, http://dx.doi.org/10.1038/srep04375.
[27] L. Guadagno, B. De Vivo, Di Bartolomeo, P. Lamberti, Tucci V. Sorrentino, et al., Effect of functionalization on the thermo-mechanical and electrical behavior of multi-wall carbon nanotube/epoxy composites, Carbon 49 (2011) 1919–1930, http://dx.doi.org/10.1016/j.carbon.2011.01.017.
[28] D. Vennerberg, Z. Rueger, M.R. Kessler, Effect of silane structure on the properties of silanized multiwalled carbon nanotube-epoxy nanocomposites, Polymer 55 (2014) 1854–1865, http://dx.doi.org/10.1016/j.polymer.2014.02.018.
[29] W. Li, C. Shi, M. Shan, Q. Guo, Z. Xu, Z. Wang, et al., Influence of silanized low-dimensional carbon nanofillers on mechanical, thermomechanical, and crystallization behaviors of poly(L-lactic acid) composites - a comparative study, J. Appl. Polym. Sci. 130 (2013) 1194–1202, http://dx.doi.org/10.1002/app.39259.
[30] J. Kathi, K.-Y. Rhee, J.H. Lee, Effect of chemical functionalization of multiwalled carbon nanotubes with 3-aminopropyltriethoxysilane on mechanical and morphological properties of epoxy nanocomposites, Compos Part A 40 (2009) 800–809, http://dx.doi.org/10.1016/j.compositesa.2009.04.001.
[31] U. Tayfun, Y. Kanbur, U. Abaci, H.Y. Guney, E. Bayramli, Mechanical, flow and electrical properties of thermoplastic polyurethane/fullerene composites: effect of surface modification of fullerene, Compos Part B 80 (2015) 101–107, http://dx.doi.org/10.1016/j.compositesb.2015.05.013.
[32] S. Halder, S. Ahemad, S. Das, J. Wang, Epoxy/Glass fiber laminated composites integrated with amino functionalized ZrO_2 for advanced structural applications, ACS Appl. Mater Interfaces 9 (2015) 1695–1706, http://dx.doi.org/10.1021/acsami.5b09149.
[33] Y. Martinez-Rubi, B. Ashrafi, J. Guan, C. Kingston, A. Johnston, B. Simard, et al., Toughening of epoxy matrices with reduced single-walled carbon nanotubes, ACS Appl. Mater Interfaces 3 (2011) 2309–2317, http://dx.doi.org/10.1021/am200523z.
[34] A. Nistal, C. Palencia, M.A. Mazo, F. Rubio, J. Rubio, J.L. Oteo, Analysis of the interaction of vinyl and carbonyl silanes with carbon nanofiber surfaces, Carbon 49 (2011) 1635–1645, http://dx.doi.org/10.1016/j.carbon.2010.12.047.
[35] L.-C. Tang, Y.-J. Wan, D. Yan, Y.-B. Pei, L. Zhao, Y.-B. Li, et al., The effect of graphene dispersion on the mechanical properties of graphene/epoxy composites, Carbon 60 (2013) 16–27, http://dx.doi.org/10.1016/j.carbon.2013.03.050.
[36] C. Wang, Z.-X. Guo, S. Fu, W. Wu, D. Zhu, Polymers containing fullerene or carbon nanotube structures, Prog. Polym. Sci. 29 (2004) 1079–1141, http://dx.doi.org/10.1016/j.progpolymsci.2004.08.001.
[37] I.D. Rosca, F. Watari, M. Uo, T. Akasaka, Oxidation of multiwalled carbon nanotubes by nitric acid, Carbon 43 (2005) 3124–3131, http://dx.doi.org/10.1016/j.carbon.2005.06.019.
[38] V. Datsyuk, M. Kalyva, K. Papagelis, J. Parthenios, D. Tasis, A. Siokou, et al., Chemical oxidation of multiwalled carbon nanotubes, Carbon 46 (2008) 833–840, http://dx.doi.org/10.1016/j.carbon.2008.02.012.
[39] B. Scheibe, E. Borowiak-Palen, R.J. Kalenczuk, Oxidation and reduction of multiwalled carbon nanotubes - preparation and characterization, Mater Charact. 61 (2010) 185–191, http://dx.doi.org/10.1016/j.matchar.2009.11.008.
[40] L.Y. Chiang, J.W. Swirczewski, C.S. Hsu, S.K. Chowdhury, S. Cameron, K. Creegan, Multi-hydroxy additions onto C_{60} fullerene molecules, J. Chem. Soc. Chem. Commun. (1992) 1791–1793, http://dx.doi.org/10.1039/c39920001791.
[41] Y. Kanbur, Z. Küçükyavuz, Synthesis and characterization of surface modified fullerene, Fullerenes, Nanotub Carbon Nanostructures 20 (2012) 119–126, http://dx.doi.org/10.1080/1536383X.2010.533306.
[42] E.A. Smith, W. Chen, How to prevent the loss of surface functionality derived from aminosilanes, Langmuir 24 (2008) 12405–12409, http://dx.doi.org/10.1021/la802234x.
[43] H.J. Martin, K.H. Schulz, J.D. Bumgardner, K.B. Walters, An XPS study on the attachment of triethoxsilylbutyraldehyde to two titanium surfaces as a way to bond chitosan, Appl. Surf. Sci. 254 (2008) 4599–4605, http://dx.doi.org/10.1016/j.apsusc.2008.01.066.
[44] J. Zhu, S. Wei, A. Yadav, Z. Guo, Rheological behaviors and electrical conductivity of epoxy resin nanocomposites suspended with in-situ stabilized carbon nanofibers, Polymer 51 (2010) 2643–2651, http://dx.doi.org/10.1016/j.polymer.2010.04.019.
[45] A.G. Osorio, I.C.L. Silveira, V.L. Bueno, C.P. Bergmann, H_2SO_4/HNO_3/HCl—Functionalization and its effect on dispersion of carbon nanotubes in aqueous media, Appl. Surf. Sci. 255 (2008) 2485–2489, http://dx.doi.org/10.1016/j.apsusc.2008.07.144.
[46] T. Sakthivel, V. Gunasekaran, S.-J. Kim, Effect of oxygenated functional groups on the photoluminescence properties of graphene-oxide nanosheets, Mater Sci. Semicond. Process 19 (2014) 174–178, http://dx.doi.org/10.1016/j.mssp.2013.12.015.
[47] N. Roy, R. Sengupta, A.K. Bhowmick, Modifications of carbon for polymer composites and nanocomposites, Prog. Polym. Sci. 37 (2012) 781–819, http://dx.doi.org/10.1016/j.progpolymsci.2012.02.002.
[48] G.V. Andrievsky, V.K. Klochkov, A.B. Bordyuh, G.I. Dovbeshko, Comparative analysis of two aqueous-colloidal solutions of C60 fullerene with help of FTIR reflectance and UV–Vis spectroscopy, Chem. Phys. Lett. 364 (2002) 8–17, http://dx.doi.org/10.1016/S0009-2614(02)01305-2.
[49] J. Zhang, H. Zou, Q. Qing, Y. Yang, Q. Li, Z. Liu, et al., Effect of chemical oxidation on the structure of single-walled carbon nanotubes, J. Phys. Chem. B 107 (2003) 3712–3718, http://dx.doi.org/10.1021/jp027500u.
[50] P.C. Ma, J.-K. Kim, B.Z. Tang, Functionalization of carbon nanotubes using a silane coupling agent, Carbon 44 (2006) 3232–3238, http://dx.doi.org/10.1016/j.carbon.2006.06.032.
[51] Y. Nie, T. Hübert, Effect of carbon nanofiber (CNF) silanization on the properties of CNF/epoxy nanocomposites, Polym. Int. 60 (2011) 1574–1580, http://dx.doi.org/10.1002/pi.3124.
[52] F. Avilés, C. Sierra-Chi, Nistal, May-Pat, F. Rubio, J. Rubio, Influence of silane concentration on the silanization of multiwall carbon nanotubes, Carbon 57 (2013) 520–529, http://dx.doi.org/10.1016/j.carbon.2013.02.031.
[53] T.H. Goswami, R. Singh, S. Alam, G.N. Mathur, Thermal analysis: a unique method to estimate the number of substituents in fullerene derivatives, Thermochim. Acta 419 (2004) 97–104, http://dx.doi.org/10.1016/j.tca.2004.02.001.
[54] S. Bhattacharya, S. Banerjee, Spectrophotometric study of complexation of benzoyl acetone with [60]- and [70] fullerenes and some other electron acceptors, Chem. Phys. Lett. 393 (2004) 504–510, http://dx.doi.org/10.1016/j.cplett.2004.06.073.
[55] T. Braun, H. Rausch, J. Mink, Raman spectroscopy of the effect of reactor neutron irradiation on the structure of polycrystalline C_{60}, Carbon 43 (2005) 870–873, http://dx.doi.org/10.1016/j.carbon.2004.10.046.
[56] B. Dongil, B. Bachiller-Baeza, Guerrero-Ruiz, I. Rodríguez-Ramos, Martínez-Alonso, J.M.D. Tascón, Surface chemical modifications induced on high surface area graphite and carbon nanofibers using different oxidation and functionalization treatments, J. Colloid Interface Sci. 355 (2011) 179–189, http://dx.doi.org/10.1016/j.jcis.2010.11.066.
[57] Z. Špitalský, C.A. Krontiras, S.N. Georga, C. Galiotis, Effect of oxidation treatment of multiwalled carbon nanotubes on the mechanical and electrical properties of their epoxy composites, Compos Part A 40 (2009) 778–783, http://dx.doi.org/10.1016/j.compositesa.2009.03.008.
[58] J.M. González-Domínguez, A. Ansón-Casaos, A.M. Díez-Pascual, B. Ashrafi, M. Naffakh, D. Backman, et al., Solvent-free preparation of high-toughness epoxy-SWNT composite materials, ACS Appl. Mater Interfaces 3 (2011) 1441–1450, http://dx.doi.org/10.1021/am101260a.
[59] J. Shen, W. Huang, L. Wu, Y. Hu, M. Ye, The reinforcement role of different amino-functionalized multi-walled carbon nanotubes in epoxy nanocomposites, Compos Sci. Technol. 67 (2007) 3041–3050, http://dx.doi.org/10.1016/j.compscitech.2007.04.025.
[60] S.G. Prolongo, M. Campo, M.R. Gude, R. Chaos-Morán, Ureña. Thermo-physical characterisation of epoxy resin reinforced by amino-functionalized carbon nanofibers, Compos Sci. Technol. 69 (2009) 349–357, http://dx.doi.org/10.1016/j.compscitech.2008.10.018.
[61] D. Vennerberg, Z. Rueger, M.R. Kessler, Effect of silane structure on the properties of silanized multiwalled carbon nanotube-epoxy nanocomposites, Polymer 55 (2014) 1854–1865, http://dx.doi.org/10.1016/j.polymer.2014.02.018.
[62] M. Abdalla, D. Dean, D. Adibempe, E. Nyairo, P. Robinson, G. Thompson, The effect of interfacial chemistry on molecular mobility and morphology of multiwalled carbon nanotubes epoxy nanocomposite, Polymer 48 (2007) 5662–5670, http://dx.doi.org/10.1016/j.polymer.2007.06.073.
[63] S. Zeng, C. Reyes, J. Liu, P.A. Rodgers, S.H. Wentworth, L. Sun, Facile hydroxylation of halloysite nanotubes for epoxy nanocomposite applications, Polymer 55 (2014) 6519–6528, http://dx.doi.org/10.1016/j.polymer.2014.10.044.
[64] T. McNally, P. Potschke, P. Halley, M. Murphy, D. Martin, S.E.J. Bell, et al., Polyethylene multiwalled carbon nanotube composites, Polymer 46 (2005) 8222–8232, http://dx.doi.org/10.1016/j.polymer.2005.06.094.
[65] A. Saritha, K. Joseph, Effect of nano clay on the constrained polymer volume of chlorobutyl rubber nanocomposites, Polym. Compos 36 (2015) 2135–2139, http://dx.doi.org/10.1002/pc.23124.
[66] P. Song, Y. Zhu, L. Tong, Z. Fang, C(60) reduces the flammability of polypropylene nanocomposites by in situ forming a gelled-ball network, Nanotechnology 19 (2008) 1–10, http://dx.doi.org/10.1088/0957-4484/19/22/225707.
[67] W. Yu, J. Fu, X. Dong, L. Chen, H. Jia, L. Shi, Highly populated and nearly monodispersed nanosilica particles in an organic medium and their epoxy nanocomposites, ACS Appl. Mater Interfaces 5 (2013) 8897–8906, http://dx.doi.org/10.1021/am402845d.